LAWRENCE
LIVERMORE
NATIONAL
LABORATORY

UCRL-TR-209420

Femtosecond, High-Brightness Electron Beam Generation and Advanced Diagnosis

S. G. Anderson, W. J. Brown, A. M. Tremaine, J. Kuba, F. V. Hartemann, D. N. Fittinghoff

February 3, 2005

This work was performed under the auspices of the U.S. Department of Energy by University of California, Lawrence Livermore National Laboratory under Contract W-7405-Eng-48.

Femtosecond, High-Brightness Electron Beam Generation and Advanced Diagnosis

S.G. Anderson, W.J. Brown, A.M. Tremaine,
J. Kuba, F.V. Hartemann, and D.N. Fittinghoff

February 14, 2005

1 Executive Summary

1.1 Abstract

This document serves as the final report for LDRD project number 04-LW-031, in which we created sub-picosecond length, kilo-amp peak current electron beams with the 100 MeV electron/positron linac, using a novel technique designed to produce ultra-short bunch lengths while maintaining the high brightness produced by the S-band photoinjector. In addition, a diagnostic to measure the temporal distribution of the beam was investigated, as conventional pulse length measurement techniques do not apply to extremely short pulses. The creation and diagnosis of beams with both femtosecond length and high transverse brightness is of major concern to next generation acceleration and radiation production experiments. This work leveraged the previous investment in the PLEIADES facility and it's ability to produce high brightness electron beams. In addition, the ultra-short electron pulses generated by this work have been used in conjunction with the PLEIADES X-ray source to produce sub-picosecond, high-brightness X-ray pulses.

1.2 Mission Relevance

This work was directly motivated by the electron beam requirements of advanced x-ray sources such as the PLEIADES Thomson scattering source [1]. As such, it was driven by key programmatic responsibilities including material studies for PDRP and diagnostics for NIF and therefore, directly aligned with the LLNL and DoE missions. In addition, the results of this work have important consequences for LLNL collaborative projects such as the Linac Coherent Light Source (LCLS) [2] and Next Linear Collider (NLC) [3]. The basic science and technology development aspects of this work made it appropriate for LDRD funding.

LLNL's 100 MeV electron/positron linac was well suited for this project, since it leveraged the significant prior investment in the production of high brightness electron beams. Besides the facilities required for this work, the Lab's considerable laser expertise was also required to produce the highest quality photo-electron beams.

1.3 Accomplishments

We have investigated an alternative electron bunch compression scheme, termed velocity bunching [4], which avoids the detrimental effects of bending magnets by using accelerator sections alone to compress and accelerate the beam; as the compression occurs in a purely linear geometry, coherent synchrotron radiation (CSR) is completely eliminated. We have utilized the velocity bunching process to create bunches with rms lengths under 300 fs and peak currents approaching one kA.

These measurements have been found to agree well with simulations. The effect of this bunching technique on the transverse beam quality and final energy spread have been directly measured to evaluate the potential of this method to produce not only ultrashort bunches, but also the extremely high-brightness beams important to the fields of radiation production and advanced accelerators. This compression technique has been applied in the PLEIADES project, resulting in a sub-picosecond X-ray source with a peak brightness over 50% greater than that produced without compression.

These efforts have produced a publication in Physical Review Special Topics: Accelerators and Beams [5] (UCRL-JRNL-207372). In conjunction with a collaborative effort between LLNL and UCLA to produce a novel, strong focusing system on the PLEIADES experiment [6], the project has lead to an invitation to speak at the 2005 Particle Accelerator Conference on the topic of ultra-high density electron beams for beam radiation and beam plasma interactions.

The successful production of sub-picosecond time scale electron bunches highlights the limitations of conventional temporal diagnostics and suggests diagnostic development as an avenue of future research. For this reason, a radio frequency (rf) deflector cavity based temporal measurement method was investigated. Modeling of such a device found it to be capable of sub-100 fs resolution and single-shot measurements of the longitudinal phase space distribution of the beam.

The project has considerably expanded the capability of the LLNL 100 MeV linac to produce and maintain femtosecond beams with very high brightness, making it a more attractive facility for radiation production, including FEL harmonics [7], nonlinear Compton scattering [8], and laser acceleration experiments [9].

2 Introduction

Recently, the demand for applications of high brightness — low emittance, high current, with sub-ps pulse length — electron beams has increased dramatically [2, 10, 11, 12]. Such applications are found in advanced accelerators; for example, the source injection requirements for short wavelength, high gradient accelerators demand ultra-short pulses of very low emittance. Additionally, relatively high charge, sub-ps electron beams are required for driving plasma wake-field accelerators. In the 4th generation synchrotron light source community, high brightness beams are needed for application to short wavelength self-amplified spontaneous emission free-electron lasers (SASE FEL), as well as for inverse-Compton-scattering (ICS) generation of short X-ray pulses.

Recent designs of systems capable of delivering high brightness very short electron beams have included the use of conventional photoinjectors in conjunction with magnetic compressors [10]. While magnetic compression schemes have proven successful in increasing the beam current, their impact on the transverse phase space has been shown not to be benign. When performing the compression at low energy, both velocity-field and centrifugal space-charge forces are not yet strongly suppressed by the relativistic cancellation of electric and magnetic fields, and their emittance-damaging effect becomes significant, during bends [13, 14]. In the case of compression at higher energy, there can be deleterious effects on the longitudinal as well as the transverse phase space of CSR [15, 16, 17, 18]. Both longitudinal and transverse phase space filamentation, and associated emittance growth, run counter to the goal of increasing the beam brightness that motivates the use of compression to begin with.

An alternative scheme that may preserve the transverse phase space quality, while compressing the beam to sub-ps bunch length, has been proposed by Serafini and Ferrario (SF) [4]. This scheme, commonly known as "velocity bunching" — as opposed to the path-length dependence of magnetic compression systems — is an extension of the commonly employed technique of RF rectilinear compression. As design trajectory bending is not needed in this system, one may avoid the phase space degrading effects observed in magnetic compression experiments on photoinjector-derived beams [13, 14]. Velocity bunching has been typically used to bunch dc electron sources at kinetic energies in the 100's of keV range. It has also been used in RF photoinjectors beginning in a similarly low-energy region very close to photocathode [19, 20] by injection of the electron bunch far ahead of the RF crest. The scheme

of SF, however, does not begin the bunching until the beam has exited the RF photocathode gun, and the initial emittance compensation (first plasma oscillation) has been completed. The bunching then occurs at energies above several MeV, during post-acceleration and the second and final transverse plasma oscillation, which produces the ultimate compensation of the emittance. The simultaneous action of velocity bunching and emittance compensation has been initially studied by SF; it is examined in further detail using simulations and experiments in this paper.

It should be emphasized that velocity bunching allows for the compression to occur early in the acceleration process, at a lower energy than magnetic compression. This attribute plays a strong motivating role for the implementation of velocity bunching in the application discussed in the following section. In the PLEIADES experiment, one simultaneously strives for short bunches, in order to achieve shorter pulse X-rays through electron beam pulse compression, and low energy spread, to obtain smaller — not as severely chromatic aberration-limited — electron beam spot sizes in the beam's final focus system. The photoinjector system in this case is an S-band RF gun, followed by four S-band traveling wave linear accelerator (linac) sections. This layout is similar in most respects to the original SF proposal, with some notable exceptions that are discussed below in the context of simulations. As the velocity-based compression occurs not within a drift, but inside of a linac, we term this variant of velocity bunching "phase space rotation", in which the synchrotron motion is mediated by continuous application of RF acceleration forces.

In order to place the present work in correct context, one must review the previous experiments in which velocity bunching has been employed in high brightness RF photoinjectors. At the BNL ATF laboratrory, bunching has been observed [19, 20] in a 1.6 cell S-band RF gun when the electron beam is launched from the cathode at phases, in standard RF gun convention, far below 90°. This effect has been shown to produce modest compression of beams, and is based on both phase space rotation within the gun, and ballistic bunching after the gun. Furthermore, it was consistent with achieving good emittance behavior. The use of this type of velocity bunching is limited, however, by the constraints simultaneously placed on the photo-emission, acceleration, focusing, and space-charge handling aspects of the system. The SF proposal allows more flexibility in velocity bunching, by moving the onset of the compression process to the entrance of the first linac section, after the initial emittance compensation. It thus separates the functions of producing an initially optimized beam, and subsequent compression. Further, in order to preserve the emittance during velocity bunching, the SF scheme proposes use of external focusing solenoids around the linac sections. This allows for tuning of the beam sizes and associated emittance oscillations during velocity bunching and post-acceleration.

Recently, a set of experiments have been performed [21] at the BNL SDL laboratory, in a layout which may approximate, from the longitudinal dynamics viewpoint, the low energy component (first two 3-m linac sections) of the SF scheme. In these measurements, agreement was found between simulation and experimental determination of the bunch length, with a minimum rms pulse length of 0.6 ps. Because no solenoid focusing was available at the SDL linac, however, the issues of transverse beam size and emittance control were not addressed experimentally.

In contrast, the LLNL phase space rotation experiments discussed here, solenoids are used to optimize the transverse emittance during the bunching process. Further, the compressed beams, having rms pulse lengths as short as 0.3 ps, are used in ICS experiments, providing a demonstration of the utility of the SF scheme of velocity bunching. It should be noted that the ATF version of velocity bunching has been used as a tool for creating shorter bunches for a variety of applications. The present results obtained at PLEIADES show much more dramatic compression in this first use of the SF velocity scheme in application than previously obtained.

3 Velocity bunching using phase space rotation

Velocity bunching, in the form initially proposed by SF, differs from a similar compression technique, termed "ballistic compression." While in ballistic compression the RF structure is used to impart

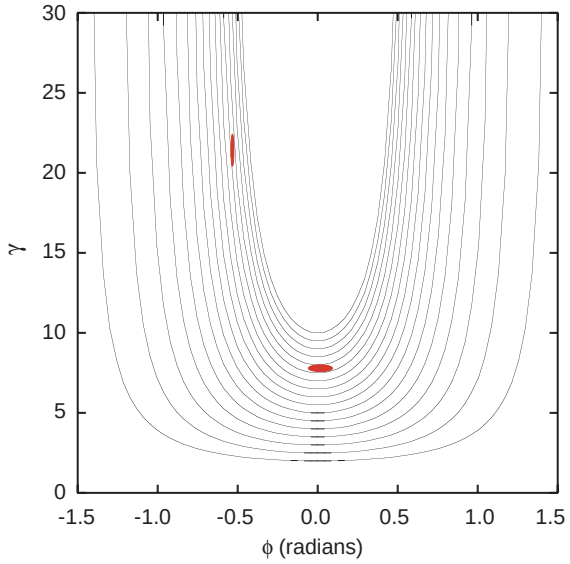

Figure 1: Longitudinal phase space particle trajectories in a traveling wave linac section modeled by a sinusoidal accelerating field. The RF parameters used in the plot are typical values for the LLNL 100 MeV linac. The plot illustrates the phase space rotation compression mechanism for a bunch injected near the RF zero crossing.

a longitudinal phase space correlation that is removed later by a drift, in the phase space rotation method, the energy/phase correlation is imparted and removed smoothly, through phase slippage and acceleration, inside of the RF linac section. In this method the beam is rotated through one quarter of a phase space oscillation, as illustrated in Fig. 1.

To understand the velocity bunching mechanism in detail, we perform an analysis similar to that of SF, but using a speed-of-light phase velocity wave, as is available at the PLEIADES linac, instead of a slow wave treatment. If one follows the arguments of SF, it can be seen that a speed-of-light phase velocity may give very close to optimum compression, as deduced from a phase space mapping analysis, which we will review below. The analysis of SF emphasizes the utility of slowing the wave phase velocity in the bunching system, in which case one may obtain a quarter-rotation of the phase space concomitant with acceleration of the beam. This idealized rotation begins with a beam having no initial phase-energy correlation, injected at the zero-crossing of the wave, and ends with maximum energy spread and minimum phase extent.

In practice, the fact that this quarter-wave rotation from the ideal initial condition is not typically achieved in a speed-of-light accelerating wave is not critical, as one may simply choose a slightly different initial RF phase to provide further rotation. Also, the tuning of the phase velocity is used in the SF scheme to change the distance along the accelerator required to obtain a quarter synchrotron oscillation. This is helpful, as in the absence of such an option, one must rely on tuning of the accelerating field amplitude alone. In practice, this concern is also mitigated, since the linac sections at PLEIADES are relatively short (2.5 m), and adjustments in the phase between sections may be used to fine-tune the acceleration scheme, in a way that is functionally equivalent to changing the phase velocity. Because of these considerations, one may view the PLEIADES setup as essentially equal in effect to the ideal case analyzed by SF. As a final comment, we note that the minimum bunch length achievable in this system is dominated by the distortion of the final phase space by the nonlinearity of the sinusoidal forces used. This effect may be mitigated by use of higher harmonic RF cavities in addition to the fundamental.

We begin our analysis by considering the (averaged over the fast fluctuations of the field occurring

in a single cell of the linac) interaction of an electron with the sinusoidal longitudinal electric field component of the RF wave in a traveling wave structure,

$$E_z = E_0 \sin(\phi) \tag{1}$$

where $\phi = kz - \omega t + \phi_0$ is, as in our discussion of the ballistic buncher, the electron phase with respect to the wave, and $k = \omega/c$ for the speed-of-light wave. Our phase convention is such that peak acceleration occurs when $\phi = -\frac{\pi}{2}$. With this electric field, the electron motion obeys a time-independent Hamiltonian (which is thus a constant of the motion) of the form:

$$H = \gamma - \sqrt{\gamma^2 - 1} - \alpha \cos(\phi), \tag{2}$$

where $\alpha \equiv eE_0/mc^2k$ is the dimensionless vector potential amplitude of the wave. The electron trajectories can be tracked and plotted in (ϕ, γ) phase space using the electron equations of motion:

$$\frac{d\gamma}{dz} = -\alpha k \sin\phi, \tag{3}$$

$$\frac{d\phi}{dz} = k\left[1 - \frac{\gamma}{\sqrt{\gamma^2 - 1}}\right]. \tag{4}$$

Examples of these phase space trajectories, which follow curves of constant Hamiltonian, are shown in Fig. 1. In this case, trajectories are plotted for typical RF parameters at the LLNL 100 MeV linac, $k = 59.8m^{-1}$, $\alpha = 0.3$ and with a minimum γ between 2 and 10.

As the plot shows, particles injected at or near $\phi_0 = 0$ will begin to slip into an accelerating phase. As the particles accelerate to ultra-relativistic velocity, the phase slippage slows, and is eventually arrested. This can be seen by using $\gamma \gg 1$ in Eq. 4, giving $d\phi/dz \cong -k/2\gamma^2$, which tends to zero sufficiently quickly for ϕ to approach a finite asymptote. The asymptotic phase limit can be found from Eq. 2 to occur when $H = -\alpha\cos\phi$. In terms of the initial conditions ϕ_0 and γ_0, the phase as $\gamma \to \infty$ is:

$$H = -\alpha\cos\phi_\infty = \gamma_0 - \sqrt{\gamma_0^2 - 1} - \alpha\cos\phi_0, \tag{5}$$

or

$$\phi_\infty \cong \cos^{-1}\left[\cos\phi_0 - \frac{1}{2\alpha\gamma_0}\right], \tag{6}$$

where, as above, the approximation $1 - \beta \cong 1/2\gamma^2$ has been used.

The phase space rotation occurs as a result of the varying orientation of the phase contour lines. If two particles are injected at $\phi_0 = 0$ with a difference in phase but no spread in energy, such that they align parallel to a phase contour, then they will remain parallel to that contour as they slip in phase and accelerate. As the particles approach ϕ_∞, their orientation becomes nearly parallel to the γ axis, having rotated by nearly 90 degrees. To evaluate the phase compression that occurs for a beam with non-zero initial phase and energy spreads, $\Delta\phi_0$ and $\Delta\gamma_0$ respectively, one can assume for simplicity that the extraction phase is ϕ_∞. In that case, expanding Eq. 6 to first order in the initial energy spread and second order in the initial phase spread gives

$$\begin{aligned}\Delta\phi_\infty = {} & \frac{\sin\phi_0}{\sin\phi_\infty}\Delta\phi_0 + \frac{1}{2\alpha\gamma_0^2\sin\phi_\infty}\Delta\gamma_0 \\ & + \frac{1}{2}\left[\frac{\cos\phi_0}{\sin\phi_\infty} - \frac{\cos\phi_\infty\sin^2\phi_0}{\sin^3\phi_\infty}\right](\Delta\phi_0)^2\end{aligned}. \tag{7}$$

Using $\Delta\gamma_0/\gamma_0 = 10^{-3}$, $\Delta\phi_0 = 4^\circ$, $\gamma_0 = 8$, $\alpha = 0.3$, and $\phi_0 = 0$ results in a final phase spread of $\Delta\phi_\infty = 0.2^\circ$, and a compression ratio of roughly 20.

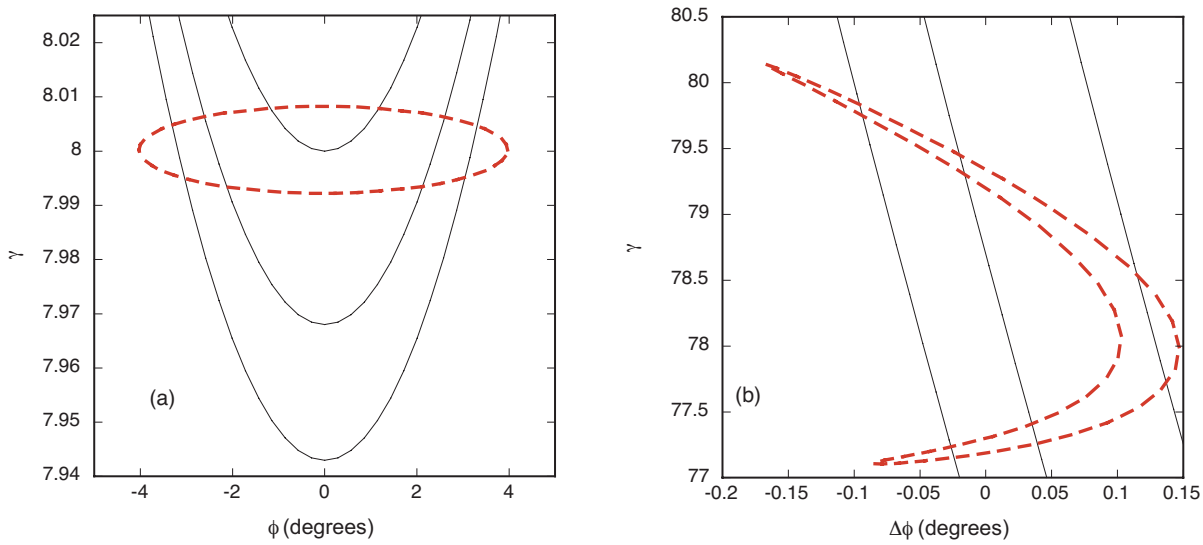

Figure 2: (a) Phase contours (solid lines) intersecting an ellipse (dashed line) representing the injected beam distribution. (b) Phase contours (solid lines) and extracted beam phase space (dashed line) obtained by integrating Eqs. 3 and 4 for points on the injected beam ellipse.

It is important to note that for this example, the $(\Delta\phi_0)^2$ term in Eq. 7 is an order of magnitude larger than the $\Delta\gamma_0$ term, thus explaining our dropping of the term proportional to $(\Delta\gamma_0)^2$. The fact that the phase spread of the injected beam limits the minimum final bunch length is a result of nonlinear RF forces increasing the longitudinal emittance of the beam. This can be understood by examining the constant Hamiltonian lines at the injection and extraction points. At $\phi_0 = 0$ the phase contours, $\gamma(\phi, H)$, have a curvature that does not follow the outline of the injected beam ellipse (using the same parameters as above). As the beam transforms under the influence of acceleration and slippage these contours "straighten out" near the asymptotic phase, forcing the initial ellipse to distort, gaining a nonlinear correlation and therefore, an increased emittance. This process is illustrated in Fig. 2, which shows the phase contours intersecting the initial beam ellipse in (a) and the same contours in (b) as the phase approaches with the resulting distorted beam shape.

4 Velocity bunching at PLEIADES

The PLEIADES facility at LLNL produces picosecond pulses of hard X-rays (10-200 keV) by colliding an ultra-relativistic electron beam (20-100 MeV) with a high intensity, 50 fs, 800 nm laser pulse. This X-ray source is designed to enable pump-probe experiments used to temporally resolve material structural dynamics on atomic time scales [12]. The PLEIADES project follows the results of previous ICS generation of sub-ps pulses of hard X-rays, demonstrated at the LBNL (Lawrence Berkeley National Laboratory) Advanced Light Source injector linac, with (30 keV) X-ray beam fluxes of 10^5 photons/pulse [22, 23]. In addition, ICS X-rays have notably been created at the Naval Research Laboratory [24] and the ATF [25], and in the γ-ray spectral region at KEK [26].

The duration of the X-ray pulse generated though this scattering process is determined by the duration of the overlap of the electron and laser beams. Thus, to produce sub-picosecond X-ray pulses desirable for pump-probe experiments, one may choose a 90° interaction geometry, in which the laser samples only part of the highly focused electron beam, or a 180° geometry, where the laser interacts with the entire electron bunch, which must be compressed to sub-picosecond length.

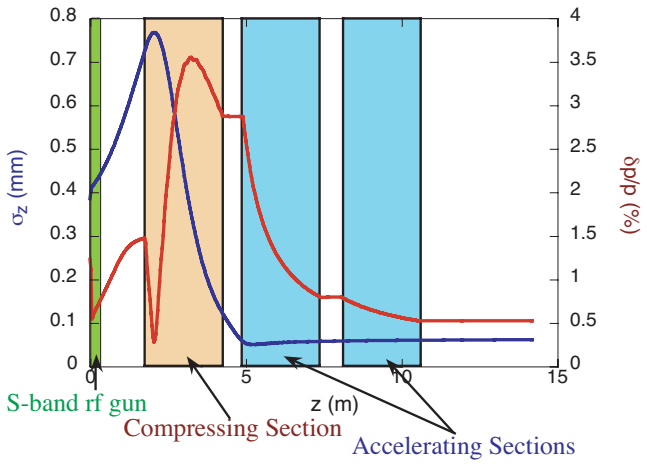

Figure 3: HOMDYN simulation of the bunch length and relative energy spread in the velocity bunching scheme implemented at PLEIADES. The bunch charge in this case is 250 pC. The rms bunch length (plotted in blue) initially increases in the drift region between the rf gun and the compressing traveling wave linac section. The majority of the compression occurs within the first linac section and the minimum bunch length, 50 µm, is achieved at the entrance to the second linac section. The rms energy spread (plotted in red) peaks at a few percent in the compressor and decreasing in the following two sections to a final value of 0.5%.

Bunch compression is therefore, an attractive option for the facility, but since the brightness of the X-ray source depends critically on the electron beam spot size ($B \propto \sigma^{-4}$), the bunching method used must be evaluated to determine if negative effects on the emittance or energy spread of the beam will reduce X-ray brightness to an unacceptable level. Velocity bunching is an obvious choice for this application, because the compression effectively occurs at low (gun exit) energy, and thus one may remove much of the energy spread that can cause unacceptable chromatic aberrations in the ICS final focus. The PLEIADES experiments thus also afford us the ability to examine effect of velocity bunching on the ICS source.

The PLEIADES photoinjector and linac consist of a 1.6 cell photo-cathode RF gun followed by four SLAC style 2.5 meter, S-band traveling wave sections. While the linac is capable of producing 100 MeV electrons, it is typically run using only the first two or three sections for X-ray production, resulting in beam energy between 20 and 70 MeV. The gun and each linac section are powered by separate klystrons, making power and phase control independent for each accelerator section. We simulated the velocity bunching process in this system using HOMDYN and PARMELA. In this case, experimental values of the accelerating gradients in the different accelerators were used in the simulations.

In Fig. 3 the pulse length and relative momentum spread evolution are simulated using HOMDYN. The gun field gradient used in this simulation was 75 MV/m (limited by RF break-down at the time of the measurements) and the charge was 0.25 nC. As the figure shows, these parameters result in significant bunch lengthening and increased energy spread after the gun. At the entrance to the compressor section, the beam correlation in longitudinal phase space is the opposite of that required for compression. It is clear from the evolution of the energy spread in Fig. 3 that this correlation is quickly reversed in the compressor, but the presence of this correlation requires a larger amount of phase space rotation in order to fully compress the beam. Consequently, it was found in these simulations that the injection phase that gives the shortest output bunches was Ð17° (*i.e.* ahead of the zero crossing). It is interesting to note that the optimal injection phase even for an idealized, uncorrelated beam was found to be about 2° forward of zero crossing. This is because the average exit phase of the beam

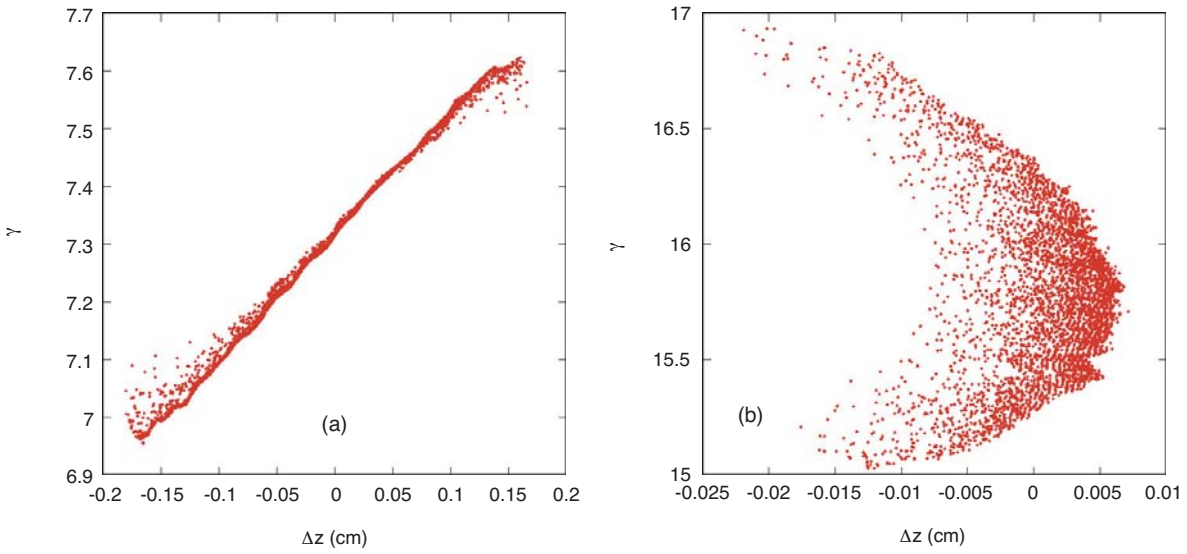

Figure 4: PARMELA simulation of the longitudinal phase space (a) before the compressing RF section and (b) after the section. A clear de-bunching correlation is present and must be removed at the beginning of the bunching section.

is not ϕ_∞, since the RF section has a finite length. The phase contours at the beam exit point have a finite slope, and injecting slightly ahead of $\phi = 0$ compensates for this slope.

Figure 4 shows the longitudinal phase space plots in PARMELA simulations for the injected and extracted electron bunches. The strong debunching phase space correlation of the injected beam is clearly evident. The simulated rms bunch duration reaches a minimum value of approximately 200 femtoseconds, and does not change significantly after the compressor. The rms relative energy spread at the end of the compressing section is 3%. In the two accelerator sections after the compressor, the beam is injected at $\phi = -\pi/2$ for maximum acceleration. Immediate acceleration of the beam is important, as it arrests the bunching process, decreases the relative energy spread, and mitigates the extremely strong transverse space-charge forces on the bunch, which at this point has 500 amps peak current and low energy ($\gamma = 16$).

The final beam energy predicted by simulation was 50 MeV. The final rms energy spread, as shown in Fig. 3 is 0.5%. The energy spread produced by simulating all three sections on crest is 0.2%, in agreement with beam measurements. This increase in energy spread is potentially problematic, since it can limit the minimum spot size achievable in ICS X-ray generation. It was found however, that emittance is the dominant factor for our experiments so that emittance growth and not energy spread is the larger concern for X-ray production.

Control of the transverse dynamics is accomplished with the solenoids that are placed around each of the traveling wave sections. Emittance growth is avoided by choosing the focusing strength of the solenoids to match the defocusing space-charge forces on the beam. This process is illustrated in Fig. 5, which shows the evolution of the horizontal spot size and normalized emittance of the beam as it compresses. The gun solenoid strength is set to match the beam into the compressor section in the manner prescribed by emittance compensation. From the compressing section the solenoid strengths are set to minimize beam size oscillations through the system. The emittance oscillations increase in frequency as the bunch compresses and subsequently slow as the beam accelerates. This is a sensitive process; the plot in Fig. 5(b) shows emittance growth caused by mismatching one of the section solenoids.

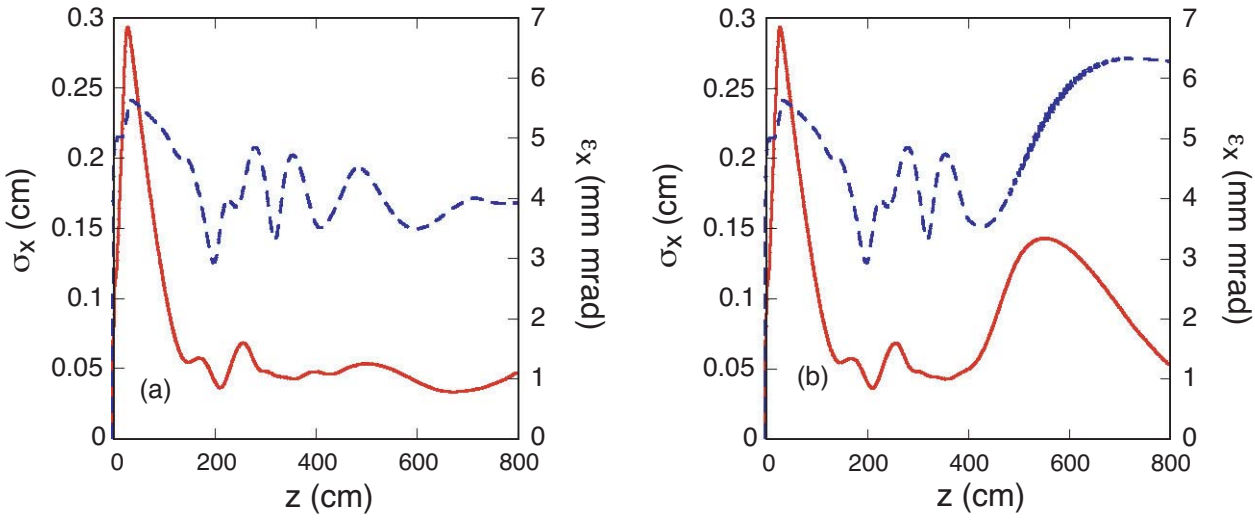

Figure 5: PARMELA simulation of the rms spot size (solid line) and normalized emittance (dashed line). In (a) the solenoid strengths are chosen to keep the beam size constant in the compressing and accelerating sections. The beam is mismatched in (b), resulting in emittance growth.

In addition to this matching sensitivity, it was also observed in the simulations that emittance growth was a very sensitive function of compression. When the beam compresses to the point of longitudinal phase space wave-breaking, the emittance compensation (or more aptly, control of oscillation) process no longer works well.

5 PLEIADES Beam Measurements

The phase space rotation method has been used in the PLEIADES system as described in the previous section. The beam and accelerator parameters were measured and used to generate the simulations shown above. Specifically, a 250 pC, 3.5 MeV bunch was generated with the 1.6 cell gun and compressed in the first of three traveling wave sections used in the experiment. The accelerating gradients of the first to last sections were 5, 10, and 10 MeV/m, respectively, with the low gradient in the first section due to low available klystron power.

As in the Neptune measurements, CTR interferometry was used to measure the sub-picosecond pulses we produced. The experimental procedure used to compress the beam was complicated by the significant variation of the phase slippage in the compressor section with injection phase. As a result, it is insufficient to change only the phase of the initial linac (compressor) section and ignore the phases of the following sections. A calculation of the dependence of phase slippage on injection phase is shown in Fig. 6; it indicates that the amount of phase slippage increase from the best acceleration phase to the best compression phase is more than 30°. Phasing the following sections appropriately must be done to properly accelerate on crest, thereby arresting the phase space rotation and minimizing the relative energy spread. The electron bunch was compressed by initially tuning the linac for highest energy. The phase of the compressor section was then set and the phases of the accelerating sections were also set using the calculation in Fig. 6 and fine tuned by maximizing the CTR detector signal. The interferometer data obtained for the shortest bunch length achieved is given in Fig. 7. The data analysis was performed using the same method as with the Neptune case; the fit gives a 300 fs rms minimum σ_t. The interferometer wire spacing issues are identical to those discussed for Neptune, and

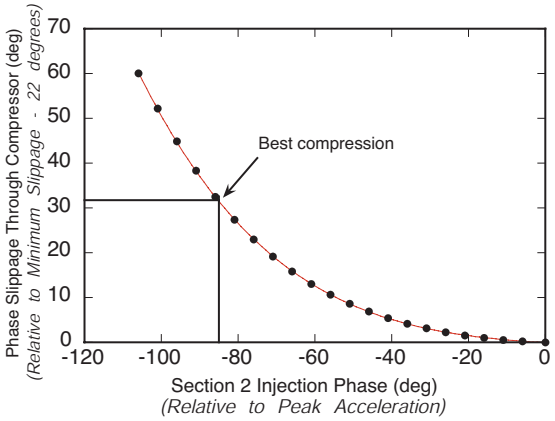

Figure 6: Model calculation of the phase slippage in the compressor as a function of injection phase. The injected phase is relative to the phase for best acceleration, 20° ahead of crest.

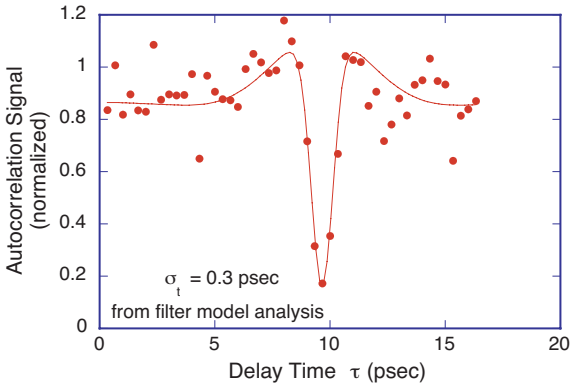

Figure 7: Autocorrelation data for the optimally compressed bunch at PLEIADES.

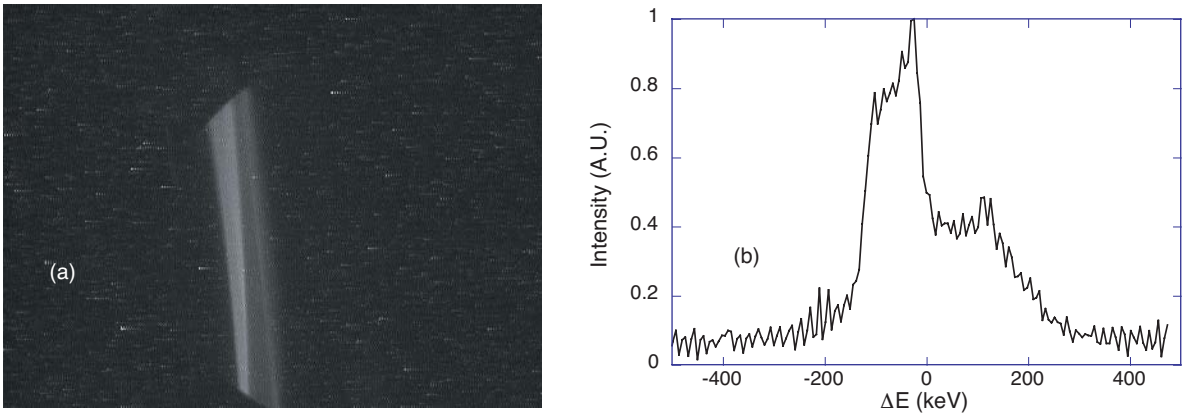

Figure 8: (a) Image of the compressed beam at the spectrometer. (b) Lineout of the image in (a). The relative, rms energy spread is roughly 0.5%.

they indicate that problems are expected for σ_t of 300 fs or below. The present measurement therefore gives an upper bound to σ_t, which is a bit longer than given in simulations (~200 fs), as seen in Fig. 3. Note also that this measurement produced even shorter beams, at similar same charge, as the Neptune case. This is most importantly due to the shorter initial pulse length (2.5 ps rms) in the PLEIADES case.

The compressor phase for strongest compression was measured at 85° ahead of the best acceleration phase, which, because of the amount of slippage through the section, is not at, but about 20° ahead of crest. This agrees well with simulations. The energy spread was measured at the linac exit using a spectrometer magnet, and found to be roughly 0.5%, as shown in Fig. 8.

For both the compressed and uncompressed electron beams, the emittance was measured using quadrupole scanning. The best emittance achieved in the uncompressed case was considerably poorer than that predicted by PARMELA. This is most likely due to: poor spatial profile of the photoinjector drive laser, observed misalignments of the section solenoids, and coupling between the x and y phase planes. The emittance was observed to be asymmetric in x and y, with best values obtained $\varepsilon_{n,x}$ =5 mm mrad and $\varepsilon_{n,y}$ =12 mm mrad. These problems make the study of emittance of the compressed beam somewhat difficult to interpret.

Nonetheless, from simulation and emittance compensation theory, we expect the emittance of the output beam to be a strong function of the focusing applied in the compressing section. Quad scan data taken with the fully compressed beam, varying the current in the first linac solenoid, is shown in Fig. 9. As expected, the emittance shows a very strong dependence on the compressor focusing, growing by a factor of 3 in $\varepsilon_{n,x}$ with a 20% change in solenoid current. A minimum of 11 mm mrad in both emittances was found to occur at the 10 A solenoid setting in this scan.

The asymmetry in the emittance of the beam results from focusing an asymmetric beam with a solenoid magnet. The initial asymmetry may be caused by an out-of-round laser spot on the photocathode, or unwanted normal and skew quadrupole fields in the gun or elsewhere. The solenoidal mixing of the coordinates x, y, x', y' of the beam particles give rise to phase space correlations in (x, y), (x, y'), and (x', y), as pointed out by Hernandez [27]. The mixing implies that $\varepsilon_{n,x}$ and $\varepsilon_{n,y}$ are no longer constants of the motion, but depending on both the amount of rotation applied by the solenoid magnets and the particulars of the down-stream optics. In fact, because these "mixed" correlations are non-zero, the 4-D phase space area is no longer given by the product, $\varepsilon_{n,x}\varepsilon_{n,y}$, but by the determinant of the full 4-D σ-matrix; $\varepsilon_{4D} = \det|\sigma|$, where the matrix element σ_{ij} is given by $\sigma_{ij} = \frac{1}{N_e}\int x_i x_j f(\mathbf{x}, \mathbf{x}')\, \mathrm{d}^2\mathbf{x}\mathrm{d}^2\mathbf{x}'$.

This effect on the emittance can be seen in the beam (either compressed or uncompressed) by

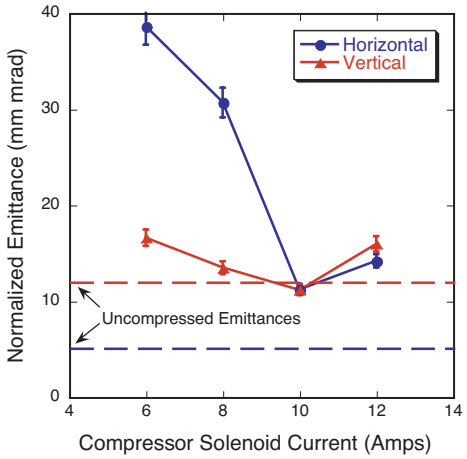

Figure 9: Measured horizontal and vertical normalized emittances of the 300 fsec beam versus the compressor solenoid strength.

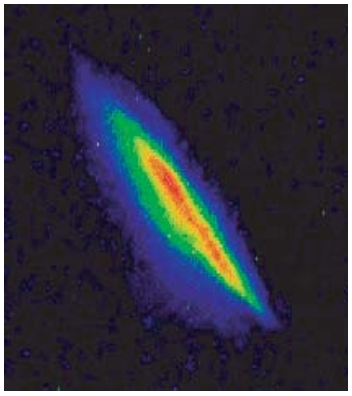

Figure 10: False color image of the electron beam showing a strong x-y correlation.

observing the (x, y) correlation, that is, by measuring σ_{13}. Figure 10 shows a typical beam at the end of the linac, in which a strong (x, y) correlation is evident. Considering this effect, a proper comparison of the compressed and uncompressed beams must examine ε_{4D}. This type of analysis follows that of Ref. [27], and is currently under development at PLEIADES. It is clear, however, based on focusability considerations in the ICS experiments, as described below, that non-negligible emittance growth occurs for the compressed beam.

6 ICS X-ray Generation With Velocity Bunched Beams at PLEIADES

While compression of electron beam to ultra-short length using velocity bunching, well shorter than in Ref. 14, is of high interest, application of this beam is perhaps more compelling. The compressed electron bunch was used in ICS experiments to generate sub-picosecond, 78 keV X-rays at PLEIADES. A schematic of the experiment is given in Fig. 11. The electron beamline consists of a two quadrupole triplets, the first used to measure the beam Twiss parameters at linac exit, and to match into the second

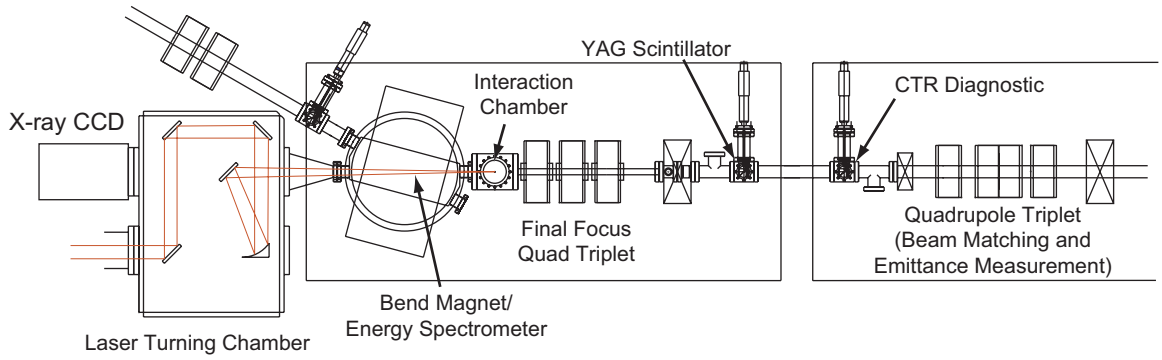

Figure 11: Schematic layout of the PLEIADES ICS X-ray source experiment.

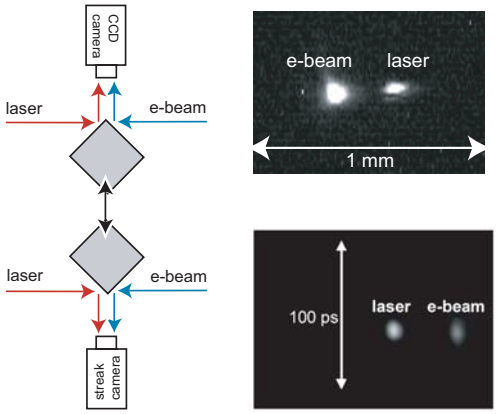

Figure 12: Illustration of the interaction point diagnostic. In one position (top) both the laser and OTR light are directed to a CCD video camera. By moving the cube transverse to the beam path, (bottom) the light is redirected to a streak camera.

set, which serve as the final focus optics before the laser-electron interaction. In addition, there are pop-in diagnostic cubes, one used to generate CTR for the bunch length diagnostic and the other to transversely image the beam. The FALCON Ti:Sapphire-based laser system delivers a 500 mJ, 50 fs (FWHM) pulse of 800 nm light to the interaction area. The laser is focused by a 1.5 m focal length off-axis parabolic lens, and directed by a final turning mirror into the 180° interaction geometry shown in Fig. 11. The X-rays generated at the interaction point propagate in the direction of the electron beam, pass through the final mirror and are detected by a CsI scintillator fiber coupled to a 16-bit CCD camera.

Two of the technical requirements of the ICS experiment are the ability to overlap the two beams spatially and temporally at the interaction point, and to achieve the highest beam densities possible at that point. These issues are addressed with a diagnostic inserted at the interaction point. A 0.76 cm, polished aluminum cube, mounted on a 3-axis translation stage, is placed in the beam path as illustrated in Fig. 12. In one position the cube reflects the (highly attenuated for measurement purposes) laser and the optical transition radiation (OTR), generated by the electron beam passing through the cube surface, out of the vacuum chamber to a CCD video camera. When the cube is translated horizontally,

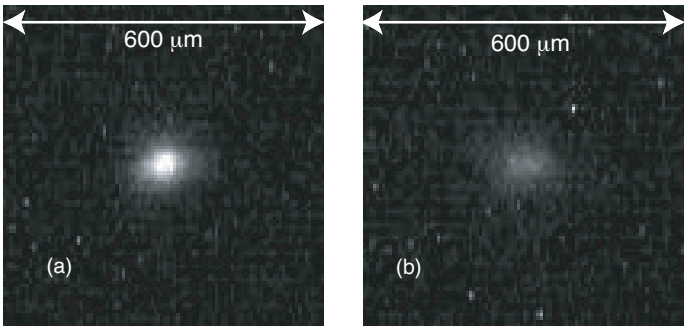

Figure 13: CCD images of the (a) uncompressed and (b) compressed electron-beam spots at the interaction point.

Table 1: RMS sizes of the compressed and uncompressed electron beams at the interaction point.

Dimension	Compressed Beam	Uncompressed Beam
x	50 μm	30 μm
y	35 μm	25 μm
z	0.1 mm	1.0 mm

the beams hit adjacent sides of the cube, and the light signals generated are redirected out the opposite vacuum port to a streak camera.

Typical optimized focused electron beam spots at the interaction point are shown for both the uncompressed and compressed cases in Fig. 13. The bunch charge in both cases was 250 pC. The compressed beam was measured to be roughly 50% larger in x and y than the uncompressed beam. The rms dimensions of both beams are given in Table 1.

Temporal overlap was accomplished by streaking the two beams at the interaction point. Streaking also allowed us to examine the timing jitter and drift of the beams. Picosecond level timing jitter is obtained at PLEIADES by using a single laser oscillator as the source that seeds both the ICS laser and the photo-cathode drive laser. The low level RF is also generated by frequency multiplying a photodiode signal from the same laser oscillator. With the RF and laser pulses synchronized in this way, the timing jitter at the interaction point has been measured to be 2 ps rms, which is at the resolution limit of the streak camera employed.

The process of bunch compression suppresses differences in injection phase, as measured with respect to the RF clock [28], demagnifying the initial laser-to-rf jitter by approximately the compression ratio. Thus because the FALCON and photoinjector drive laser are nominally locked, the tendency of the photoelectron beam to be locked to the RF clock by compression should increase the electron beam/FALCON laser jitter. The compressed bunch was streaked at the interaction point in order to measure this effect. An analysis of three different sets of streak camera images, each set taken a few minutes apart, was performed and the result is shown in Fig. 14. The shot-to-shot jitter was found to be 2-4 psec rms, which was slightly higher than that obtained with the uncompressed beam. More impressively, the laser and electron beam timing drifted noticeably over time, an effect not seen with uncompressed electrons. This drift was observed to be as large as 35 psec, and occurred on a time scale of several minutes. The phase of the gun and each of the TW sections in the linac are measured and feedback loops are in place to prevent phase drift on a time scale longer than a second. The observed time-of-flight drift may be due to slow drifts in the klystron power output feeding the compressor section, which is not controlled by a feedback loop. This drift affects X-ray production

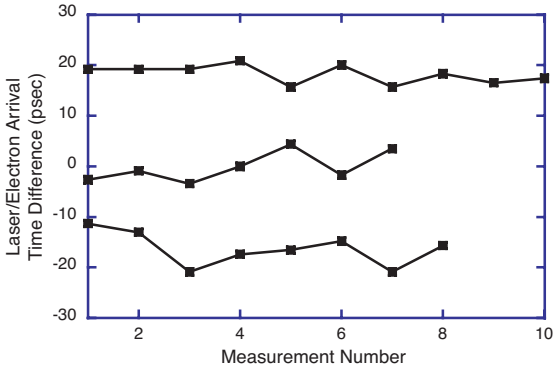

Figure 14: Laser to electron beam timing jitter measurements taken at three different times. The shot-to-shot jitter is 2-4 psec while the total drift from the two extreme data sets is 35 psec.

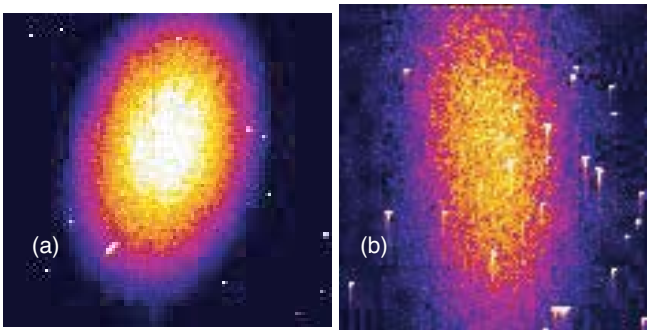

Figure 15: Single shot, false-color X-ray beam images measured by the CCD for the (a) uncompressed and (b) compressed electron beams. The color scale has yellow as most intense, with violet as lowest non-negligible intensity observed.

in the uncompressed case as well, since it alters the beam energy, thereby affecting the steering and focusing of the electrons at the interaction point.

To produce X-rays, the energy of the compressed electron beam was increased to 58 MeV by increasing the amount of RF power in the final TW section. This was done to match the energy obtained under normal conditions, and therefore produce the same X-ray wavelength. Doing this makes the comparison of X-ray data simpler since it removes the energy dependence of the laser turning mirror attenuation and the calibration of the X-ray CCD (see Fig. 11). The bunch length and emittance dynamics are not affected significantly by increasing the energy in this way.

The ICS X-rays were measured with the X-ray CCD camera for both the compressed and uncompressed beams. Figure 15 shows single shot X-ray beam data in these two cases. The number of X-ray photons can be derived from the CCD images and in the uncompressed case this number is 5×10^6 γ/pulse. For the compressed beam, a factor of 4-5 fewer photons were observed, yielding approximately 10^6 γ/pulse. When the CCD camera is integrated over many shots the ratio of normal-to-compressed X-rays increases. This is most likely a result of the timing drift discussed above.

The degradation of X-ray photon yield with velocity-bunched beam is due to the loss of electron beam focusability, which arises because of both emittance growth, and final focus chromatic aberrations that increase in importance with the enhanced energy spread of a velocity-bunched beam. At the present

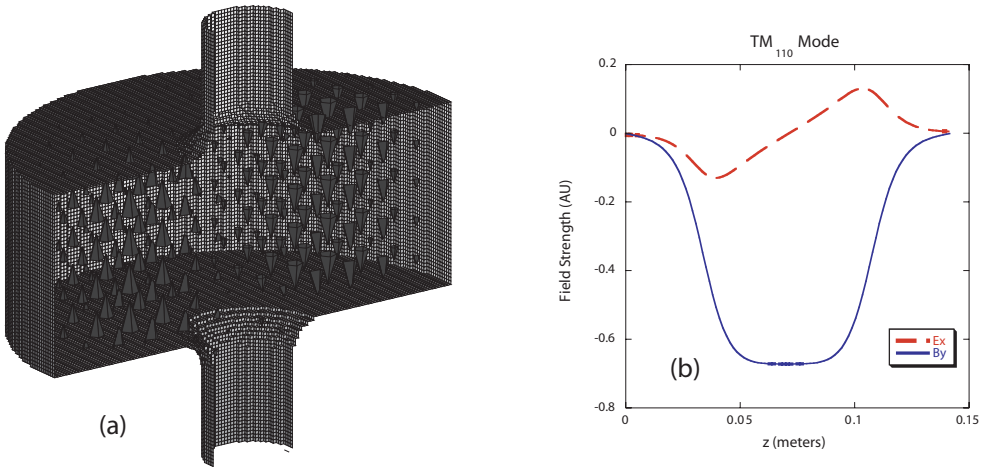

Figure 16: (a) GDFIDL simulation of the electric field of the TM110 mode of a cylindrical cavity (only half of the cavity is shown here). (b) On-axis deflecting field amplitudes of the same cavity mode.

time, the electron beam final focus has been upgraded to an extremely short focal length, permanent magnet quadrupole-based system [6]. This improvement allows the mitigation of chromatic aberrations while lowering the minimum β-function at focus, thus giving the potential to obtain much smaller spots. Much smaller spot sizes have been obtained with this system, but not as yet with velocity bunching deployed.

7 Pulse Length Measurement

As mentioned above, proven fast diagnostics are inadequate for measuring the 100 fs bunches we create using velocity bunching. Therefore, we examine a short pulse measurement device based on a transverse rf deflection cavity [29].

The operating principle of this device is similar to that of velocity bunching. The time dependent rf fields of a cavity are used to put a longitudinal correlation on the bunch. In this case, the correlation is between longitudinal position within the bunch and *transverse* momentum. This is accomplished by operating the cavity in a mode such that the field components on the beam axis are transverse (either E_x and B_y or E_y and B_x) instead of longitudinal, as is the case for an accelerating structure. After exiting the cavity the beam is allowed to drift. In the drift region the beam spreads and at the end one has the original beam longitudinal profile mapped into a transverse dimension.

One possible cavity design is illustrated in Fig. 16a. Here the electric field configuration of the TM110 mode of a cylindrical cavity is shown in the result of a simulation using the code GDFIDL [30]. As the figure shows, the accelerating (and decelerating) electric fields of this mode are off-axis. The on-axis fields in this case are B_y, and E_x, as shown in part b of the figure. In this example the cavity dimensions are chosen such that the TM110 mode resonates at the linac frequency, and so that a speed of light particle traverses the cavity in π phase advance. Note also, that the phase of the electric field is shifted by $\pi/2$ with respect to that of the magnetic field. Thus, the maximum ($+x$) electron deflection occurs when it enters the cavity as the electric field is positive but decreasing, crosses the cavity midpoint at the peak of the magnetic field, and exits while the electric field is again positive (since it's direction has changed sign). The resulting kicks of the two field components add in this configuration. The sinusoidal time dependence of the fields transfers directly to the to the particle momentum so that $p_x = p_{max} \sin\Psi$.

Using this cavity model and assuming a peak electric field of 100 MV/m, the maximum deflection of a 50 MeV beam is 42 mrad. If run at the rf zero crossing, this leads to a resolution of 0.75 mrad/rf degree, or after a meter of drift, approximately 750 μm/picosecond. The minimum beam spot size, σ_r, is limited by its emittance, and to good approximation is given by $\sigma_r \simeq L\varepsilon/\sigma_0$, where L is the drift length, ε the emittance, and σ_0 the beam size at the cavity. Assuming a normalized emittance of 5 mm mrad, and a 2 mm spot size in the cavity, the emittance limited beam size is 25 μm, rms, giving a temporal resolution of 33 femtoseconds.

We note here that a very promising design exists [29], in which two perpendicularly oriented cavities are phased in quadrature. In this case the total deflection takes the form: $x\cos\Psi + y\sin\Psi$. Thus, particles entering with the same energy will be deflected to the same radius, while particles entering at the same phase will go to the same angle. In other words, the longitudinal phase space (y,Ψ) is mapped to the transverse space (r,θ). In this way, it is possible to make a single shot longitudinal phase space measurement.

8 Conclusions

The concept of phase space rotation-based velocity bunching has been discussed here in the context of the PLEIADES injector, which is employed in ICS experiments at LLNL. This system is similar to the original proposal of SF, with the exception of the use of speed-of-light phase velocity. It was shown, through Hamiltonian analysis and HOMDYN simulations, that the slow-wave linacs emphasized by SF are not critically necessary, especially for the relatively short (2.5 m) low gradient linac sections. The PLEIADES injector system is outfitted with independently powered solenoids, allowing emittance control, which was shown to be both imperfect in effectiveness and sensitive to envelope injection mismatch. The multi-particle PARMELA simulations we employed have shown that the emittance control is nonetheless manageable until one compresses to the onset of longitudinal cross-over effects.

In experiments at PLEIADES a bunch length of $\sigma_t = 0.3$ psec was achieved; a factor of 2 shorter than that observed in a similar scenario at BNL SDL [21]. The PLEIADES measurement is near the minimum resolvable pulse length of the CTR interferometer used, and is thus consistent with the predictions of simulation and instrument resolution. Achieving this pulse length is accompanied by moderate emittance growth, which, along with chromatic aberrations, produce an increase in final spot size. Emittance control dependent on a focusing solenoid surrounding the compressor accelerating section, a critical component of the SF scheme, was demonstrated for the first time.

Based on these techniques, we have unequivocally shown the utility of the velocity bunching process for producing a decrease in X-ray pulse length, and an increase in photon brightness from the PLEIADES ICS. This spot size increase causes the yield to decline by a factor of 4, while the peak current rises by over a factor of ten. To put the overall performance of PLEIADES experiment in perspective, the peak photon flux from the BNL ATF ICS experiment was measured to be 2.2×10^{18}/sec (with 8×10^{18}/sec to be deduced from experimental efficiency estimates); after compression, PLEIADES produces 1.4×10^{18} photons/sec. We note that the ATF result was obtained partially by use a very large number of incident laser photons; the PLEIADES result is based upon obtaining peak electron current — 340 A, as opposed to 140 A at the ATF experiments.

The performance of the PLEIADES system was limited by poor initial emittance in the beam after the gun, x-y coupling, by misalignment of the focusing solenoids, and by drifts in the RF system. Efforts are underway to improve all of these experimental characteristics, in order to achieve velocity-bunched beam spots as small as 10 μm rms using the new permanent-magnet quadrupole (PMQ) final focus system. The short focal lengths of the PMQ final focus allows the mitigation of chromatic aberrations which also afflicted the present PLEIADES experiments.

Acknowledgement

This work was performed under the auspices of the U. S. Department of Energy (DOE) by the University of California, Lawrence Livermore National Laboratory (LLNL) under contract No. W-7405-ENG-48. The project (04-LW-031) was funded by the Laboratory Directed Research and Development Program at LLNL.

References

[1] G. P. LeSage, S. G. Anderson, T. E. Cowan, J. K. Crane, T. Ditmire, *et al.* In *Advanced Accelerator Concepts: Ninth Workshop*, edited by P. L. Colestock and S. Kelley, AIP Conf. Proc. No. 569 (AIP, New York, 2001).

[2] The LCLS Design Study Group. "Linac coherent light source (lcls) design study report." Technical Report SLAC Report No. SLAC-R-0521, Stanford Linear Accelerator Center (1998).

[3] International Study Group. "International study group progress report on linear collider development." Technical Report SLAC-R-559, Stanford Linear Accelerator Center (2000).

[4] L. Serafini and M. Ferrario. In *Physics of, and science with, the X-Ray Free-Electron Laser*, volume 581 (AIP Conf. Proc., 2001).

[5] S. G. Anderson, P. Musumeci, J. B. Rosenzweig, W. J. Brown, R. J. England, *et al.* "Velocity bunching of high-brightness electron beams." *Phys. Rev. ST Accel. Beams*, **8**, p. 014401 (2005).

[6] J. Lim, P. Frigola, J.B. Rosenzweig, S. Telfer, G. Travish, *et al.* In *Proceedings of the 2003 Particle Accelerator Conference*, p. 2192 (IEEE, 2003).

[7] A. Tremaine, X. J. Wang, M. Babzien, I. Ben-Zvi, M. Cornacchia, *et al.* "Experimental characterization of nonlinear harmonic radiation from a visible self-amplified spontaneous emission free-electron laser at saturation." *Phys. Rev. Lett.*, **88**, p. 204801 (2002).

[8] F. V. Hartemann and A. K. Kerman. "Classical theory of nonlinear compton scattering." *Phys. Rev. Lett.*, **76**, p. 624 (1996).

[9] A. L. Troha, J. R. Van Meter, E. C. Landahl, R. M. Alvis, Z. A. Unterberg, *et al.* "Vacuum electron acceleration by coherent dipole radiation." *Phys. Rev. E*, **60**, p. 926 (1999).

[10] J. B. Rosenzweig, N. Barov, and E. Colby. "Pulse compression in rf photoinjectors: Applications to advanced accelerators." *IEEE Trans. Plasma Sci.*, **24**, p. 409 (1996).

[11] C. E. Clayton and L. Serafini. *IEEE Trans. Plasma Sci.*, **24**, p. 400 (1996).

[12] S. G. Anderson, C. P. J. Barty, S. M. Betts, W. J. Brown, J. K. Crane, *et al.* "Short-pulse, high-brightness x-ray production with the pleiades thomson-scattering source." *Appl. Phys. B*, **78**, p. 891 (2004).

[13] H. Braun, R. Corsini, L. Groening, F. Zhou, A. Kabel, *et al.* "Emittance growth and energy loss due to coherent synchrotron radiation in a bunch compressor." *Phys. Rev. ST Accel. Beams*, **3**, p. 124402 (2000).

[14] S. G. Anderson, J. B. Rosenzweig, P. Musumeci, and M. C. Thompson. "Horizontal phase-space distortions arising from magnetic pulse compression of an intense, relativistic electron beam." *Physical Review Letters*, **91**, p. 074803 (2003).

[15] John S. Nodvick and David S. Saxon. *Phys. Rev.*, **96**, p. 180 (1954).

[16] K. Ishi, Y. Shibata, T. Takahashi, H. Mishiro, T. Ohsaka, *et al. Phys. Rev. A*, **43**, p. 5597 (1991).

[17] S. Heifets, G. Stupakov, and S. Krinsky. *Phys. Rev. ST Accel. Beams*, **5**, p. 064401 (2002).

[18] S. Reiche and J. B. Rosenzweig. *Phys. Rev. ST Accel. Beams*, **6**, p. 040702 (2003).

[19] X. J. Wang, X. Qiu, and I. Ben-Zvi. *Phys. Rev. E*, **54**, p. R3121 (1996).

[20] X. J. Wang. In *Proceedings of the 1999 Particle Accelerator Conference*, p. 229 (IEEE, 1999).

[21] P. Piot, L. Carr, W. S. Graves, and H. Loos. *Phys. Rev. ST Accel. Beams*, **6**, p. 033503 (2003).

[22] R. W. Schoenlein, W. P. Leemans, A. H. Chin, P. Volfbeyn, T. E. Glover, *et al.* "Femtosecond X-ray Pulses at 0.4 A Generated by 90° Thomson Scattering: A Tool for Probing the Structural Dynamics of Materials." *Science*, **274**, pp. 236 (1996).

[23] W. P. Leemans, R. W. Schoenlein, P. Volfbeyn, A. H. Chin, T. E. Glover, *et al.* "X-ray based subpicosecond electron bunch characterization using 90¡ thomson scattering." *Phys. Rev. Lett.*, **77**, p. 4182 (1996).

[24] A. Ting, R. Fischer, A. Fisher, C. I. Moore, B. Hafizi, *et al.* "Demonstration experiment of a laser synchrotron source for tunable, monochromatic x-rays at 500 ev." *Nucl. Instrum. Methods Phys. Res., Sect. A*, **375**, p. ABS68 (1996).

[25] I. V. Pogorelsky, I. Ben-Zvi, T. Hirose, S. Kashiwagi, V. Yakimenko, *et al.* "Demonstration of 8×10^{18} photons/second peaked at 1.8 Å in a relativistic Thomson scattering experiment." *Phys. Rev. ST Accel. Beams*, **3**, p. 090702 (2000).

[26] I. Sakai, T. Aoki, K. Dobashi, M. Fukuda, A. Higurashi, *et al.* "Production of high brightness gamma rays through backscattering of laser photons on high-energy electrons." *Phys. Rev. ST Accel. Beams*, **3**, p. 090702 (2000).

[27] M. E. Hernandez. Ph.D. thesis, Stanford University (2003).

[28] J. B. Rosenzweig and G. P. LeSage. In *Advanced Accelerator Concepts Eighth Workshop Conference Proceedings*, volume 472, p. 795 (AIP, 1999).

[29] J. Haimson, B. Meeklenburg, G. Stowell, and B. Ishii. "A circularly polarized beam deflector for direct measurement of ultra short electron bunches." In *Advanced Accelerator Concepts: Tenth Workshop*, p. 810 (2002).

[30] W. Bruns. "Gdfidl: A finite difference program with reduced memory and cpu usage." In *Proceedings of the 1997 Particle Accelerator Conference*, p. 2651 (IEEE, Piscataway, NJ, 1997).